Kinetics of the Peritectic Phase Transformation: *In-Situ* Measurements and Phase Field Modeling

DOMINIC PHELAN, MARK REID, and RIAN DIPPENAAR

An experimental study has been conducted into the role of cooling rate on the kinetics of the peritectic phase transformation in a Fe-C alloy. The interfacial growth velocities of the peritectic phase transformation were measured *in situ* for cooling rates of 100, 50, and 10 K/min. *In-situ* observations were obtained using high-temperature laser scanning confocal microscopy (HTLSCM) in a concentric solidification configuration. The experimentally measured interface velocities of the liquid/austenite (L/γ) and austenite/delta-ferrite (γ/δ) interphase boundaries were observed to increase with higher cooling rates. A unique finding of this study was that as the cooling rate increased, there was a transition point where the L/γ interface propagated at a higher velocity than the γ/δ interface, contrary to the findings of previous researchers. Phase field modeling was conducted using a commercial multicomponent, multiphase package. Good correlation was obtained between model predictions and experimental observations in absolute values of interface velocities and the effect of cooling rate. Analysis of the simulated microsegregation in front of the L/γ and γ/δ interfaces as a function of cooling rate revealed the importance of solute pileup. This microsegregation plays a pivotal role in the propagation of interfaces; thus, earlier modeling work in which complete diffusion in the liquid phase was assumed cannot fully describe the rate of propagation of the L/γ and δ/γ interfaces during the course of the peritectic transformation.

I. INTRODUCTION

THE peritectic transition in iron-carbon alloys, where $L + \delta \rightarrow \gamma$, is an extremely complex and challenging phase transformation to study either experimentally or mathematically. Kerr *et al.*[1] have defined the peritectic transition into two separate components: the peritectic reaction and the peritectic transformation. The peritectic reaction occurs under the conditions where all three phases (L, δ, and γ) are in contact, and the liquid and delta-ferrite phases react to form austenite. This reaction is rapid, currently accepted to be controlled by diffusion of solute in liquid, so that a film of austenite quickly separates the liquid and delta-ferrite phases. From this point onward, further formation of austenite is defined as the peritectic transformation, and it is this aspect of the phase transition that is the focus of the current study.

Experimental difficulties in studying the peritectic transformation are related to the elevated temperatures at which this phase transformation occurs in Fe-C alloys, and hence the difficulty in making quality *in-situ* observations. Therefore, experimental studies have mostly relied upon quench experiments combined with post-transformation metallography. For example, Matsuura *et al.*[2] used a solid/liquid diffusion couple to study the kinetics of this transformation in iron-carbon alloys. The volume fractions of liquid, austenite, and delta-ferrite phases were analyzed following quenching of the diffusion couple, and the segregation of carbon was determined using an electron probe mass analyzer. The reliance upon post transformation metallography in Fe-C alloys is hampered by subsequent austenite decomposition that masks the higher temperature transformation, rendering it impossible to determine precisely the spatial history of the L/γ and γ/δ interfaces. In an alternative approach, El-Bealy and Fredriksson[3] used a chill apparatus to measure heat flow as a means to benchmark their model of the peritectic reaction, but also in this case the use of techniques to measure bulk thermal response cannot separate the spatial history of the L/γ and γ/δ interfaces during the peritectic transformation.

Recently, an experimental technique has been developed that enables high-resolution *in-situ* observation at elevated temperatures of phase transitions, including the peritectic transformation. High-temperature laser-scanning confocal microscopy (HTLSCM) was developed by Emi and his colleagues and has been used to study solidification, delta-ferrite to austenite transformations, and austenite decomposition phase transformations.[4–9] Shibata *et al.*[9] have used the HTLSCM experimental technique to make the first reported *in-situ* observations of the peritectic reaction and transformation in Fe-0.14 pct C and Fe-0.43 pct C alloys. Quantification of the kinetics of the peritectic transformation was conducted for cooling rates between 1 and 20 K/min. The growth kinetics of the 0.42 pct C alloy was found to follow a parabolic growth rate, decaying with time, consistent with diffusion-controlled growth. The growth velocities at a cooling rate of 1 K/min were determined to be 1.33 and 1.83 μm/s for the L/γ and γ/δ interfaces, respectively. The 0.14 pct C alloy, on the other hand, was found to have a transformation rate too rapid to be explained by carbon diffusion control for cooling rates up to 20 K/min. The growth rate of austenite into delta-ferrite was found to be higher than the growth rate of austenite into the liquid in both the alloys studied. In the current study, HTLSCM has also been used to study the influence of cooling rate on the kinetics of the peritectic transformation.

Mathematical modeling of microstructural development accompanying the peritectic transformation has, in the past,

DOMINIC PHELAN, APD Fellow, MARK REID, Research Associate, and RIAN DIPPENAAR, Professor, are with the Faculty of Engineering, BHP Steel Institute, University of Wollongong, NSW, Australia. Contact e-mail: phelan@udw.edu

Manuscript submitted September 5, 2003.

been limited by the high computational requirements of sharp interface models, and the lack of sufficient computational resources. As a consequence, simplifying assumptions have been made to reduce computing requirements. A common simplifying assumption is that there is complete solute mixing in the liquid phase, and this assumption is frequently extended to the delta-ferrite phase as well. For example, El-Bealy and Fredriksson[3] as well as Matsuura *et al.*[10] assumed uniform carbon distribution (complete mixing) in both the liquid and delta-ferrite phases. Das *et al.*[11] undertook a numerical study of the peritectic transformation in Cd-Ag and Pb-Bi alloys (where $L + \beta \rightarrow \alpha$), assuming complete mixing in the liquid phase but also taking into account the more rigorous case of diffusion in the alpha phase. Shibata *et al.*[9] and Won and Thomas[12] modeled the segregation during casting of Fe-C alloys of peritectic composition under the assumption of complete liquid mixing, and Ha and Hunt[13] did the same for the peritectic Ag-14 wt pct Sn alloy. These simplifying assumptions are typically justified by the argument that the rate of diffusion in the delta-ferrite and liquid phases are substantially higher than that in the austenite phase, and can therefore be neglected. The development of phase field models, a finite interface method, has significantly reduced computational requirements while maintaining physical relevance. As such, it is now possible to conduct multiphase, multicomponent simulations based on free energy minimization incorporating diffusion in all phases in a nonprohibitive time frame. Lee *et al.*[14] used a phase field model to study the peritectic reaction; their modeling domain consisted of a one-dimensional diffusion couple, both isothermal and with continuous cooling, and a two-dimensional model of the peritectic reaction, taking into account diffusion in all phases. A finding common to all these studies is that during the peritectic transformation, the growth of the δ/γ interface proceeds at a much higher rate than that of the L/γ interface.

II. EXPERIMENTAL

In-situ experimental observations of the peritectic transformation in an iron-carbon alloy were made using HTLSCM (Figure 1). Samples are placed in a gold-plated ellipsoid infrared heating furnace in an ultra-high-purity inert atmosphere, >99.9999 pct Ar. A 1.5 kW-halogen lamp located at one focal point of the cavity heats the specimen, located at the other focal point, by radiation. A quartz plate separates the specimen and lamp chambers so that the atmosphere of the specimen chamber can be controlled, to prevent oxidation, while the lamp is air cooled. The temperature, measured by thermocouples incorporated in the crucible holder, is displayed on a monitor and simultaneously recorded with the image on videotape or DVD at a rate of 30 frames per second. Hard copies of the video frames can be made or they can be subjected to digital video analysis on a computer. Specimens were held in an alumina crucible in a 10-mm-diameter round holder constructed from a polymeric end piece, alumina 2-bore tube with an outer silica support tube and a platinum holder welded to a B-type thermocouple wire. Magnifications up to 1350 times at a resolution of 0.25 μm can be obtained, using a He-Ne laser with a wavelength of 632.8 nm. In the system used, a laser beam 0.5 μm in diameter is reflected and scanned by an acoustic optical deflector in the horizontal direction at a rate of 15.7 kHz and a galvano-mirror in the vertical direction at 60 Hz.[16]

Samples were arranged in the so-called concentric solidification technique, where a radial temperature gradient is imposed on a 10-mm-diameter sample with a thickness in the range 100 to 300 μm. A detailed description of the concentric solidification configuration has been accepted for publication,[17] but a schematic representation of the thermal gradient across a specimen is shown in Figure 2 for clarity. In brief, this configuration provides a number of experimental advantages over techniques previously used. Most important are the minimization of the meniscus of the melt, resulting in a larger area that is in sharp focus across the solid/liquid interface, and the elimination of a temperature gradient in the through thickness direction. Other benefits of this configuration are that the peritectic transformation can be followed over long periods of time without the need for constant refocusing and, very importantly, that the observations made are not of surface effects only but are representative of bulk behavior.

The chemical analysis of the Fe-C alloy used is given in Table I. Specimens were heated to 1673 K at a rate of 100 K/min, and then slowly heated to a temperature where a liquid

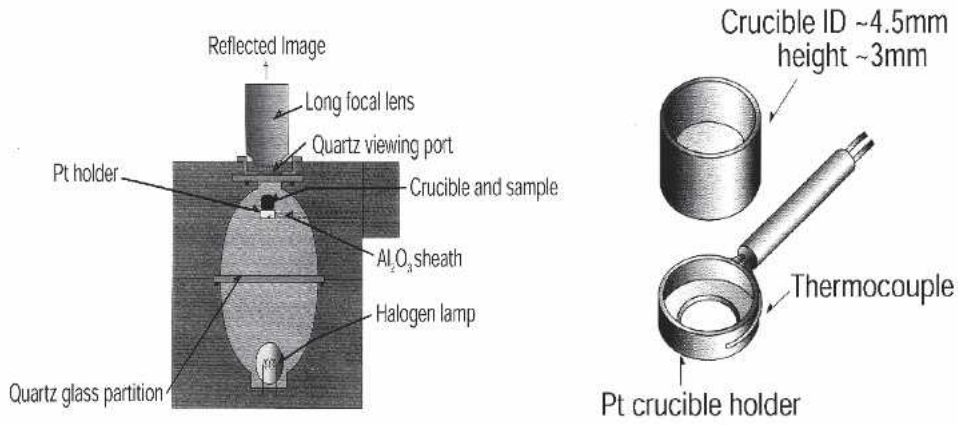

Fig. 1—Schematic diagram of the LSCM furnace and sample holder.

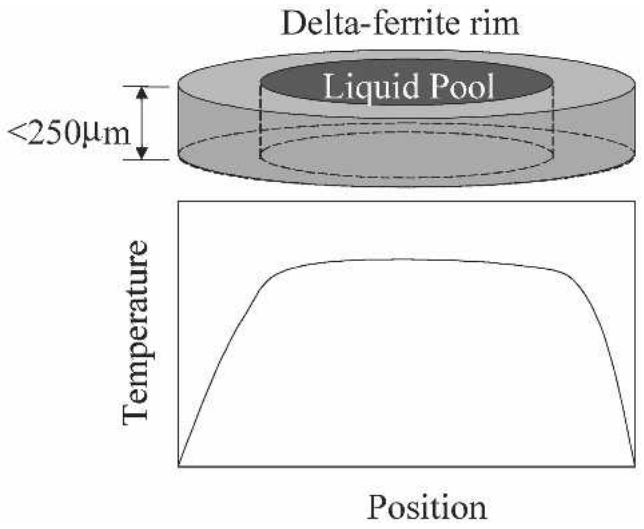

Fig. 2—Schematic of the concentric solidification setup, and corresponding temperature distribution.

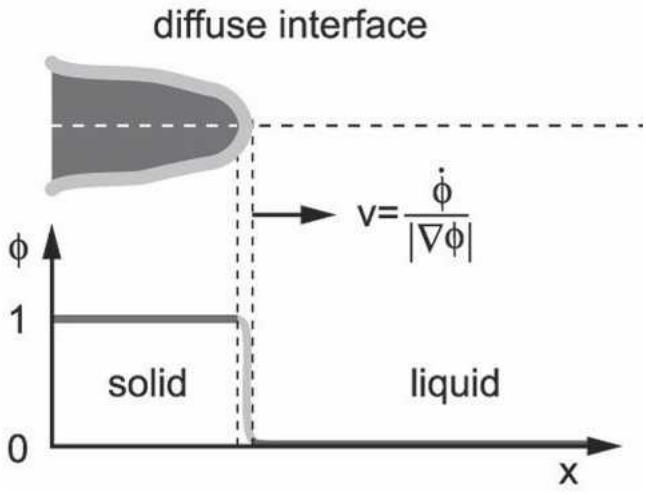

Fig. 3—Schematic representation of the treatment of an interface in the phase field model.[20]

Table I. Composition of the Fe-C Alloy

Element	C	P	Mn	Si	S	Al
Wt pct	0.18	0.002	<0.1	<0.005	0.002	0.034

pool initiated. Typically, a period of 2 minutes was required to stabilize the liquid pool, to maximize the uniformity of the pool shape, and so to ensure that the solid/liquid interface was at equilibrium and subject to the same thermal conditions at all points around the circumference of the pool. Specimens were then cooled at controlled rates of 10, 50, or 100 K/min and the progression of the delta-ferrite/liquid interface on solidification was followed with time until the peritectic reaction followed by the peritectic transformation was observed and recorded. By using frame-by-frame breakdown, the growth velocities of the delta-ferrite/liquid, liquid/austenite, and austenite/delta-ferrite interfaces were measured using image analysis software.

III. MODEL SIMULATIONS

A. *Phase Field Model*

In an attempt to better understand the experimental observations of the progress of the liquid/δ, liquid/γ, and γ/δ interphase boundaries under different cooling rates, a phase field model was employed to assess specific aspects of the experimental results. Simulations of the peritectic transformation were conducted using Micress, a multicomponent/multiphase commercial simulation software package, based on the model developed by Steinbach *et al.*[18] Tiaden[19] has previously shown that this software can be used to simulate peritectic phase transitions, although the simulation was not benchmarked against experimental measurements.[20] In the present simulations, three phases, liquid, delta-ferrite, and austenite, and one dissolved component, carbon, were modeled. In phase field models, each phase or grain is described by an order parameter, ϕ, which describes the state of the phase and is governed by the minimization of free energy functional, $\hat{f}$, as described by Steinbach *et al.*[18] (Eq. [1]). Interfaces are defined as regions of finite thickness, η, across which the order parameter changes continuously from one region to the next. This treatment is shown schematically in Figure 3, where the value of the phase field parameter varies from 1 to 0 across the solid/liquid interface.[20] The introduction of such a parameter simplifies the boundary conditions of the simulation as the entire domain can be treated as a continuum and not as a Stefan problem with a sharp interface between two distinct phases.

$$\hat{f} = \sum_{i,k(i<k)}^{n} \hat{f}_{ik} = \left[\frac{\varepsilon_{ik}^2}{2} |\phi_k \nabla\phi_i - \phi_i \nabla\phi_k|^2 + \frac{1}{4a_{ik}} \left[\phi_i^2 \phi_k^2 - m_{ik} \left(\frac{1}{3}\phi_i^3 + \phi_i^2 \phi_k - \frac{1}{3}\phi_k^3 + \phi_k^2 \phi_i) \right] \right] \quad [1]$$

ε_{ik} is defined as the gradient energy coefficient of phases i and k, m_{ik} is the linear coefficient of deviation from thermodynamic equilibrium. The terms ε_{ik}, m_{ik}, and a_{ik} are related to the interface mobility, surface tension, interface thickness, the latent heat of the phase transition, and the equilibrium transformation temperature (μ_{ik}, σ_{ik}, η_{ik}, L_{ik}, and T_{ik}, respectively) by Eqs. [2] through [4].

$$\varepsilon_{ik}^2 = \eta_{ik} \sigma_{ik} \quad [2]$$

$$m_{ik} = \frac{6 a_{ik} L_{ik} (T_{ik} - T)}{T_{ik}} \quad [3]$$

$$a_{ik} = \frac{\eta_{ik}}{72 \sigma_{ik}} \quad [4]$$

A set of kinetic equations, Eqs. [5] and [6], are developed describing the phase field parameter and solute distribution in space and time, and hence how the microstructure develops with time. In Eq. [5], the inherent mobility of interfaces, μ, is a fitting parameter used to describe interfaces that

exhibit anisotropy of mobility, for example, coherent *vs* incoherent interfaces in solid-state transformations. The influence of curvature on microstructural development is handled in Eq. [5] by the first group of terms incorporating the interfacial energy, σ_{ij}. Chemical thermodynamics is incorporated into Eq. [5] by the second group of terms, relating interface thickness, η, entropy of fusion, ΔS_{ij}, and the equilibrium undercooling, ΔT_{ij}.

$$\phi_i(\bar{x},t) = \sum_j \mu_{ij}\left[\sigma_{ij}\left(\phi_i\nabla^2\phi_j - \phi_j\nabla^2\phi_i + \frac{\pi^2}{2\eta^2}(\phi_i - \phi_j)\right) + \frac{\pi}{\eta}\sqrt{\phi_i\phi_j}\circ S_{ij}\circ T_{ij}\right] \quad [5]$$

The kinetics of the phase transformation is not determined by the minimization of the free energy functional alone, but in combination with the kinetics of solute diffusion. The phase field equations are coupled to a solute balance through the equilibrium undercooling, as defined in Eq. [6]. The solute distribution is assumed to be under local equilibrium partition conditions, with the provision that concentrations deviate from equilibrium values as a function of curvature or kinetic undercooling. Interfaces are assessed as regions of phase mixing, and the solute balance is maintained by equating the equilibrium solute distribution in each phase at a sharp interface, with a proportional contribution of each phase as determined by the phase field parameter change across a finite interface. Linearized phase diagrams are used to describe the equilibrium solute conditions for all phases being simulated and a finite difference technique is used to solve the equations, conserving the solute concentration.

$$\dot{c}_{(\bar{x},t)} = \nabla\left(\sum_{i=1}^{n}\phi_i D_i \nabla\left(k_{iR}\, c_R\right)\right) \quad [6]$$

where D_i is the diffusion coefficient of the solute in phase i, k is the partition coefficient for an interface of curvature R, and c_R is the equilibrium solute concentration for an interface of radius R.

B. *Simulation Parameters*

Whereas the preceding description of phase field modeling was of a generic nature, attention will now be given to the practicalities of modeling the peritectic phase transformation. The first step in establishing such a simulation is to provide a thermodynamic framework on which to base the calculations. To this end, linearized phase diagrams of the alloy system need to be determined. In this study, the Fe-C alloy system is described by a reference temperature (T_0), a reference solute concentration (C_0) in each phase at that temperature, and the slopes of the liquidus, solvus, and solidus (m) through the reference point. These data were generated by the software package Thermocalc (Thermo-Calc Software, Stockholm, Sweden), and the corresponding quantitative values are shown in Table II. With this linearized phase diagram, shown schematically in Figure 4, the equilibrium solute concentration in each phase can be determined for any specific alloy composition and domain temperature.

The remaining data required to describe the simulation are the entropy of transformation and the diffusion coefficient of solute in each phase, as the microstructure develops as a function of both free energy minimization and solute diffusion. The interfacial energies of the three types of phase boundaries in this simulation are also incorporated, playing a role in the morphological stability of the relevant interfaces. The diffusion and interfacial energy values were taken from the literature and are presented in Table III.

An important issue in the use of phase field models is the specific procedure followed to incorporate the interface mobility factor, μ, into the calculations. The mobility factor is a numerical construct that has no direct physical meaning, and as such, the selection of a value for this parameter can be quite arbitrary. In the model developed by Lee *et al.*,[14] a constant value for the mobility factor is assigned for the entire

Table II. Thermodynamic Data

Parameter	Value	Unit	Reference
T_o reference temperature	1792.4962	K	Thermocalc
Entropy of transformation	0.95924	kJ/m^3 K	Thermocalc
C_o (L) carbon	0.1600	wt pct	Thermocalc
C_o (δ) carbon	0.02695	wt pct	Thermocalc
m (L) carbon	−79.811157	K/wt pct	Thermocalc
m (δ) carbon	−474.45819	K/wt pct	Thermocalc
T_o reference temperature	1786.1559	K	Thermocalc
Entropy of transformation	1.0440	kJ/m^3 K	Thermocalc
C_o (L) carbon	0.160	wt pct	Thermocalc
C_o (γ) carbon	0.0478726	wt pct	Thermocalc
m (L) carbon	−61.3670	K/wt pct	Thermocalc
m (γ) carbon	−199.691	K/wt pct	Thermocalc
T_o reference temperature	1764	K	Thermocalc
Entropy of transformation	0.09157	kJ/m^3 K	Thermocalc
C_o (δ) carbon	0.0742706	wt pct	Thermocalc
C_o (γ) carbon	0.14070	wt pct	Thermocalc
m (δ) carbon	705.591	K/wt pct	Thermocalc
m (γ) carbon	436.854	K/wt pct	Thermocalc

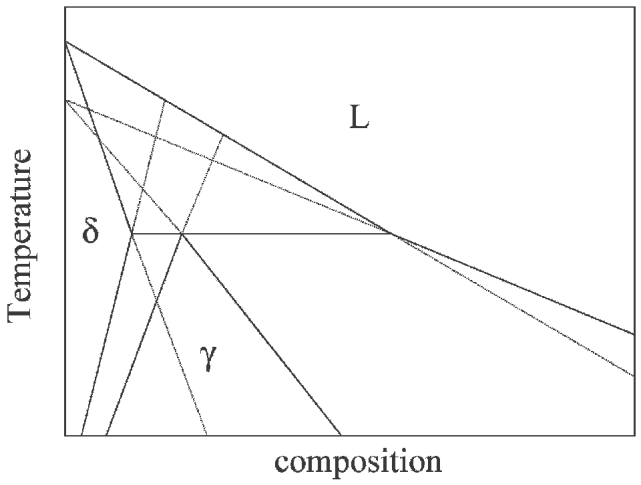

Fig. 4—Schematic of the applicable portion of the linearized Fe-C phase diagram.

Table III. Material Data

Parameter	Value	Unit	Reference
Diffusion C in liquid	2.0×10^{-8}	m^2/s	21
Diffusion C in delta	3.95×10^{-9}	m^2/s	4
Diffusion C in austenite	1.0×10^{-9}	m^2/s	21
σ_L/δ	2.04×10^{-9}	J/m^2	21
σ_L/γ	2.04×10^{-9}	J/m^2	21
σ_δ/γ	3.7×10^{-9}	J/m^2	4

simulation. The mobility factor therefore behaves as a fitting parameter and the simulation is subject to the arbitrary nature of setting this parameter. In our study, the mobility factor is not fixed but is incorporated as a continuously adjusted parameter for the case of diffusion-controlled transformations. In the simulation of the peritectic transformation, the value of the mobility factor is adjusted at each time-step such that the calculated interface velocity is consistent with diffusion-controlled conditions, thereby distinguishing the present analysis from the model used by Lee *et al.*[14]

IV. RESULTS

The experimental results of primary interest in this study are those involving the propagation of the L/δ interface during the initial cooling period, followed by the progression of the L/γ and γ/δ interfaces during the peritectic transformation. The effect of cooling rate on the propagation velocity and morphology of these interfaces as observed using HTLSCM will be presented in this section. These results will subsequently be discussed in relation to the modeling work, in Section V.

A. *Solidification—L/δ Propagation*

The L/δ interface for each cooling rate was tracked from the start of cooling until the initiation of the peritectic reaction. Observations typical of those obtained using HTLSCM are presented in Figure 5 for a cooling rate of 100 K/min. The arrows in the second frame denote the progression of the L/δ interface. Measurement of this distance with time leads to the determination of the growth velocity. In this figure, taken at the highest cooling rate, the L/δ interface has a planar morphology, and for the lower cooling rates, the L/δ interface during the initial cooling period was also observed to be planar.

B. *Peritectic Transformation*

Observations of the peritectic reaction and transformation in the Fe-C alloy studied are reproduced for cooling rates of 10, 50, and 100 K/min in Figures 6 through 8 respectively. The progression of the peritectic transformation over a period of three frames is recorded for cooling rates of 10 and 50 K/min in Figures 6 and 7, corresponding to the time-steps 0, 0.1, and 2 seconds.

In Figure 6 at $t = 0$ seconds, the L/δ interface has a planar morphology. It exhibits the characteristic alignment of δ grain boundaries in the direction of the heat flow. At $t =$ 0.1 seconds, γ has grown along the L/δ interface in the intervening time and into the δ phase. The morphology of the γ/δ in the interface is irregular with very prominent γ lathes growing into the central δ grain. Growth into the liquid phase cannot be resolved at this stage. At $t = 2$ seconds, growth of γ into the liquid phase is measurable and is observed to be much less than the growth of γ into δ. Due to the irregular morphology of the γ/δ interface, only an estimated average value of the growth rate can be obtained.

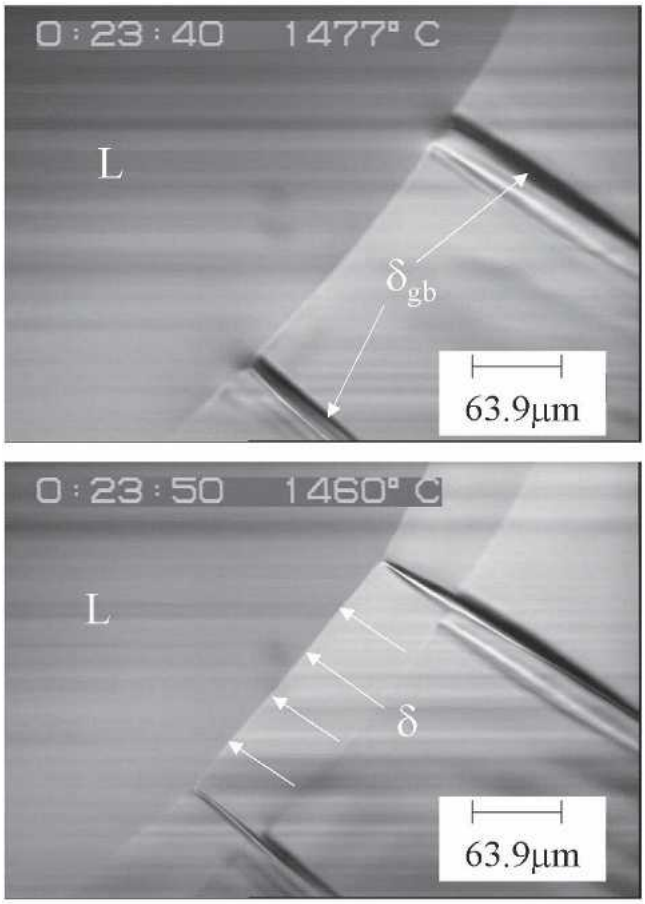

Fig. 5—Typical LSCM observations of solidification leading up to the initiation of the peritectic transition (cooling rate = 100 K/min). The first frame shows the liquid/δ interface at the commencement of cooling. The liquid phase, denoted by L, occupies the left of the frame and the δ phase occupies the right. During the isothermal hold period, the L/δ interface has stabilized presenting a curved line across the frame due to the radial nature of the thermal gradient. Two δ grain boundaries run perpendicular to the L/δ interface, having aligned in the direction of the heat flow during grain growth. In the second frame, taken 10 seconds after commencement of cooling, the L/δ interface has moved to the left, denoted by the arrows. The original position of the L/δ interface can still be observed due to thermal etching of the interface during the hold period that has resulted in the development of a groove.

In Figure 7, a time sequence equivalent to that in Figure 6 is shown for a cooling rate of 50 K/min. The sequence of events is similar to those shown in Figure 6, with the primary differences being the increase in growth velocities and the sharpening of the γ/δ interface morphology. The growth rate of γ into the δ phase is higher than that of austenite into the liquid phase.

With a further increase in the cooling rate to 100 K/min, a significant change in the sequence of events is observed (Figure 8). In this figure, two frames are recorded, $t = 0$ seconds and t = 0.3 seconds. The significant difference in comparison to the previous two cases is that the growth rate of γ into the liquid phase is very rapid, much greater than the

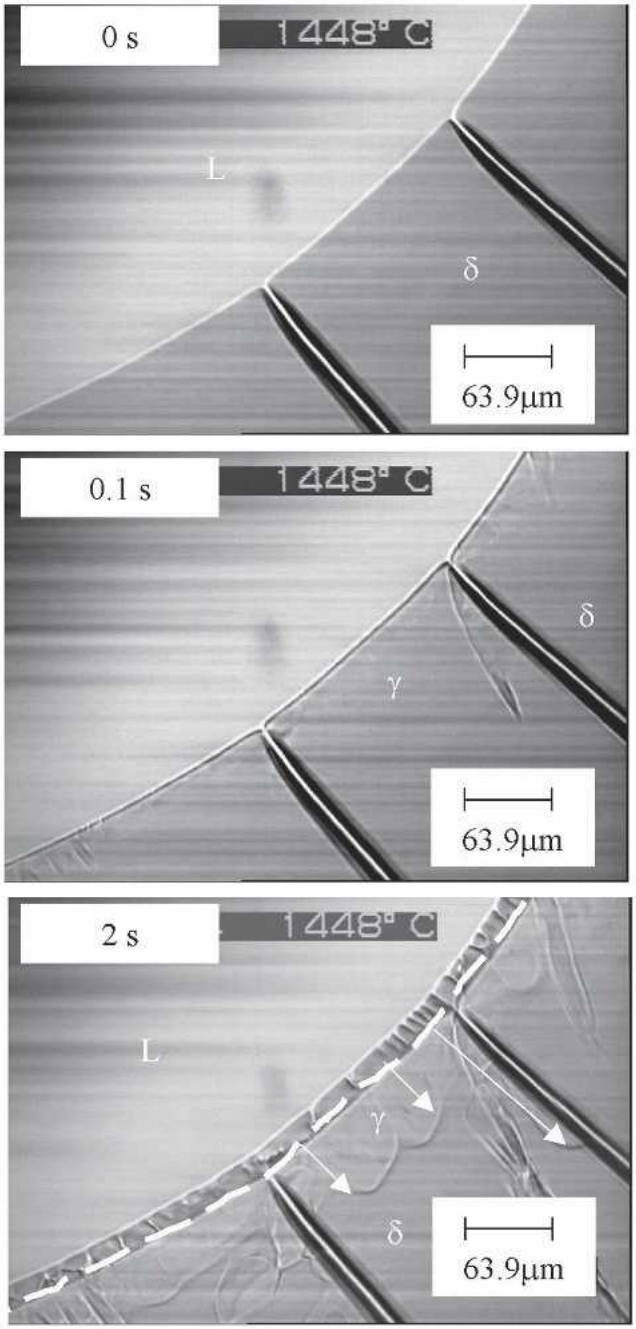

Fig. 6—Peritectic reaction and transformation in Fe-0.18 pct C alloy: cooling rate = 10 K/min, LSCM images. The superimposed broken line in the frame $t = 2$ s corresponds to the position of the L/δ interface at $t = 0$ s.

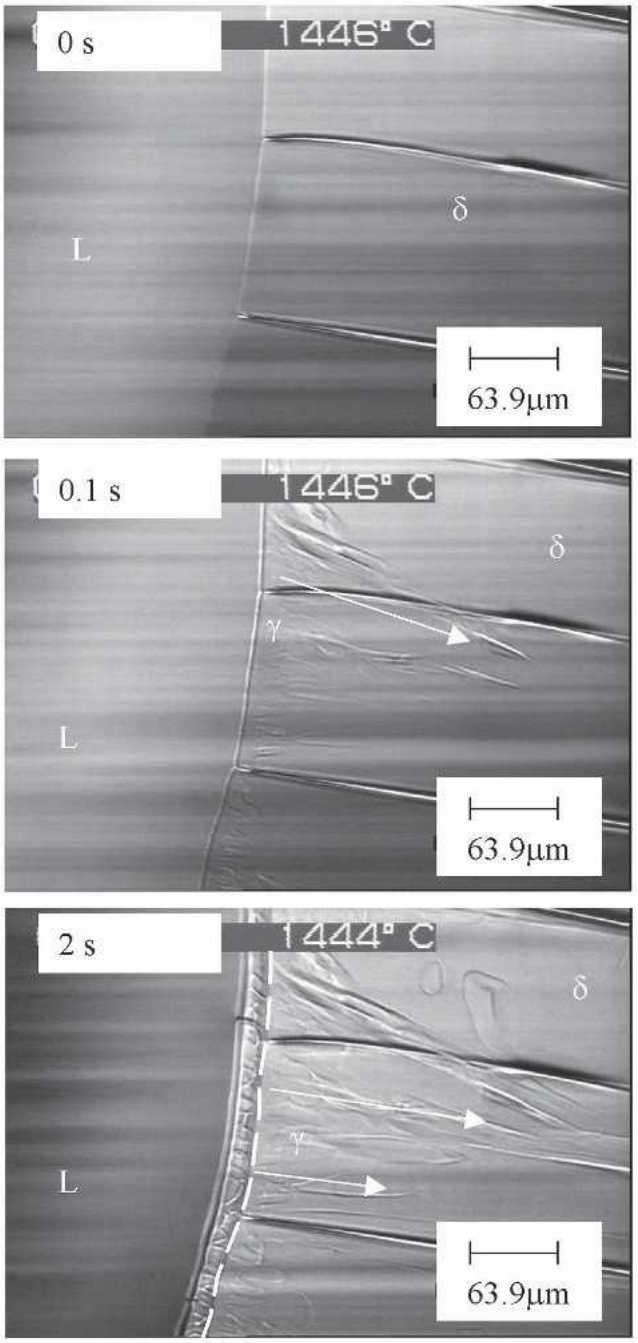

Fig. 7—Peritectic reaction and transformation in Fe-0.18 pct C alloy: cooling rate = 50 K/min, LSCM images. The superimposed broken line in frame $t = 2$ s corresponds to the position of the L/δ interface at $t = 0$ s.

growth rate of γ into the δ phase. The best estimates from the initial time period are that $V_{L/\gamma} = 900$ μm/s and $V_{\gamma/\delta} = 100$ μm/s. Unfortunately, the growth into the liquid has propagated below the focal plane; hence, the image in this instance has a poor contrast.

To display the growth of γ into the liquid phase more clearly, Figure 9 has been included. This image was taken at a later time, after refocusing on the region of austenite that has grown into the liquid. The microstructure revealed is one of cellular morphology, thus confirming that the growth rate was rapid, such that the L/γ interface was destabilized to grow with a cellular morphology. Further assessment of the interface velocities was limited due to the rapid propagation of the interfaces. However, at $t = 3.4$ seconds, the velocity of the γ/δ interface had slowed to 40.5 μm/s, while the velocity of the L/γ interface at $t = 9$, 13.3, and 28.3 seconds was measured as 54, 16.5, and 10.5 μm/s, respectively. This indicates that the growth velocities decay with time, and that at $t = 9$ seconds, the velocity of the L/γ interface is still greater than that of the γ/δ interface.

The observation of an apparent inversion in the relative growth velocities between the L/γ and γ/δ interfaces is intrigu-

ing. Previous studies that have attempted to measure or model the peritectic transformation in the Fe-C system have consistently determined that the growth rate of austenite into the delta-ferrite phase is greater than that into the liquid phase.[8,10,13]

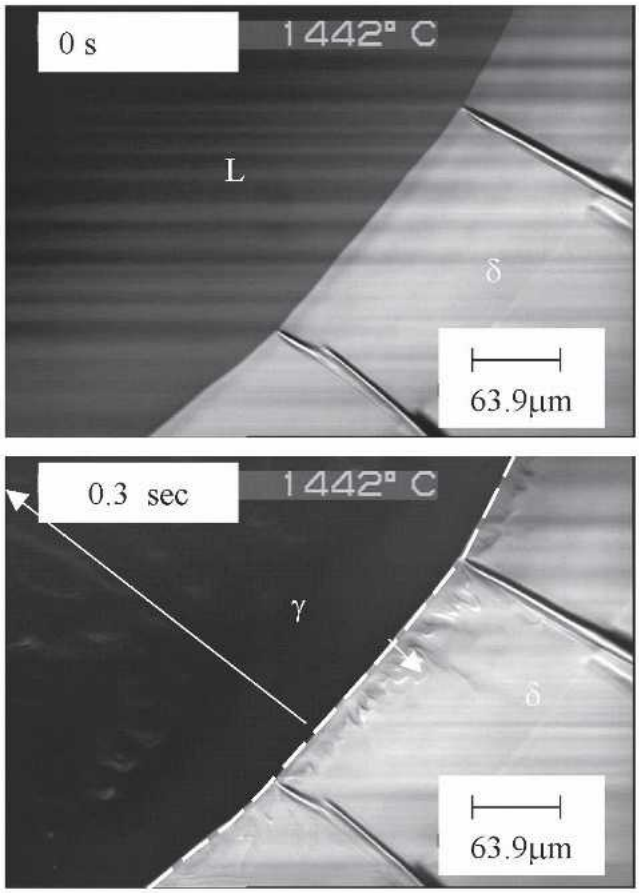

Fig. 8—Cellular growth morphology of the L/γ interface during the peritectic transformation in Fe-0.18 pct C alloy: cooling rate = 100 K/min, LSCM images. The arrows indicate the relative amount of liquid and delta-ferrite consumed by austenite in the first 0.1 seconds of the peritectic transformation.

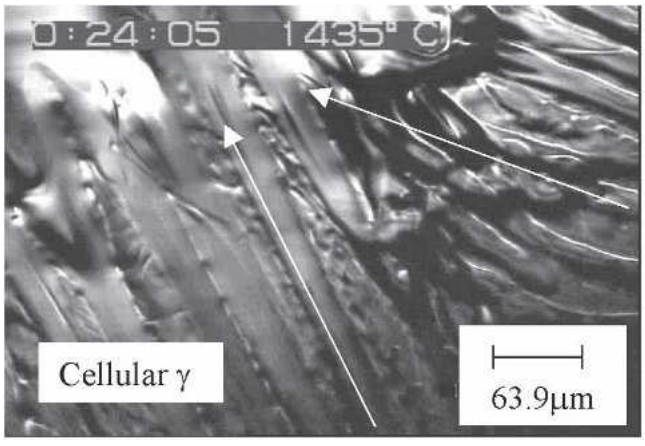

Fig. 9—Morphology of the austenite that has grown into the liquid phase in Figure 8. The arrows highlight the growth direction of two separate γ grains indicating there were two distinct nucleation events at the L/δ interface.

In order to probe this phenomenon further, a study was undertaken using phase field modeling of the directional solidification of Fe-C alloy under a specified thermal gradient. Because it was possible to accurately measure the propagation velocities of the L/γ interface over long periods of time for cooling rates of 10 and 50 K/min, these results will be used to provide a benchmark for the modeling studies conducted.

V. DISCUSSION

A. *Growth of Delta-Ferrite Prior to the Peritectic Reaction*

In Figure 10, the experimentally determined growth rate of the delta-ferrite/liquid interface is shown on cooling through the two-phase (δ + L) field at a rate of 10 K/min until the initiation of the peritectic reaction. The predicted growth rates under the same conditions are also shown in the figure. As expected, there is a transient period following the commencement of cooling where the growth velocity initially increases before the solute profiles stabilize. This first transient period is followed by a second transient regime where the growth rate decays with time as solute segregates to the liquid phase. It is evident that the model predictions are in good agreement with the experimentally determined growth behavior of delta-ferrite from the commencement of cooling to the initiation of the peritectic transition.

Whereas Figure 10 shows that the calculated rate of formation of δ from the liquid corresponds closely with experimental observations at a low cooling rate (10 K/min), there is some concern regarding the fact that the simulations are restricted to a rectangular domain whereas the experiments are based on a circular domain. In the experiments, a radial thermal gradient is imposed on the specimen, leading to the establishment of a circular melt pool. It is currently not possible to replicate the radial thermal gradient shown in Figure 2, in the simulation package, and we are restricted to a simulation domain of only a segment of the melt pool, as shown in Figure 11. A consequence of this necessary compromise is that the solute profiles in the simulation will be different from the experiment. It is to be expected that solute would segregate more in the experiment than in the

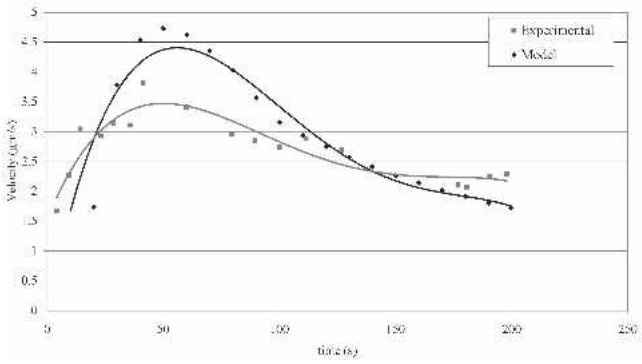

Fig. 10—Comparison of experimentally determined and model predictions of the delta/liquid interface velocity from the commencement of cooling from a temperature just below the liquidus to the initiation of the peritectic reaction. Cooling rate = 10 K/min.

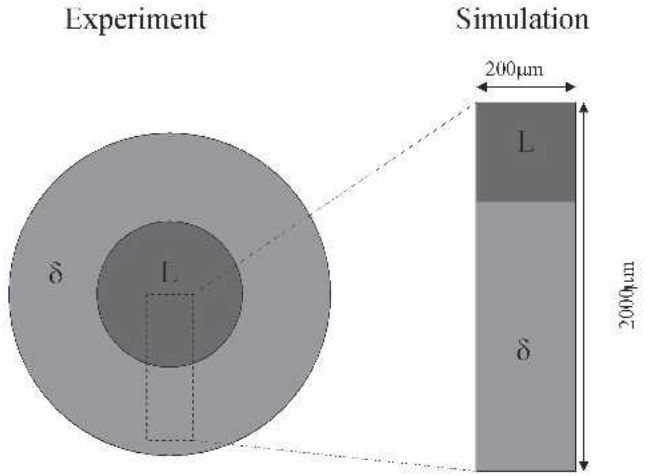

Fig. 11—Schematic representation of experimental and simulation setup.

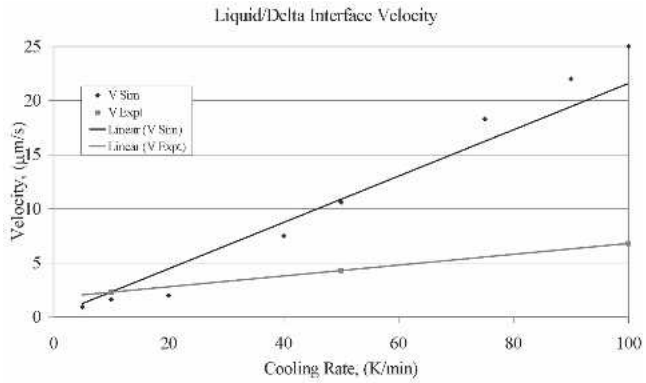

Fig. 12—Comparison of simulated and experimental measurements of the solidification velocity of the L/δ interface as a function of cooling rate.

planar simulation domain. The direct consequence is that growth velocities in the simulation will be overestimated.

For this reason, the experimentally determined L/δ interface velocities immediately preceding the peritectic reaction were compared to model predictions as a function of cooling rate and this comparison is shown in Figure 12. While both the simulated and measured growth velocities exhibit an increase with cooling rate, there is a divergence between the simulation and experimental results at higher cooling rates. The calculated growth velocity of the L/δ interface closely approximates observed measurements at low cooling rates, but at a cooling rate of 100 K/min, the experimentally measured growth rate is 7 μm/s while the simulation predicts a growth rate of 25 μm/s. This discrepancy is most probably due to the simplified simulation domain compared to the experimental setup, as explained previously. It is evident that the simulation domain more closely approaches a directional solidification experiment.

B. *Austenite/Liquid Interface Velocity during the Peritectic Transformation*

In Figures 13 and 14, a comparison is drawn between the experimentally observed and simulated growth velocities of the austenite/liquid interface following the peritectic

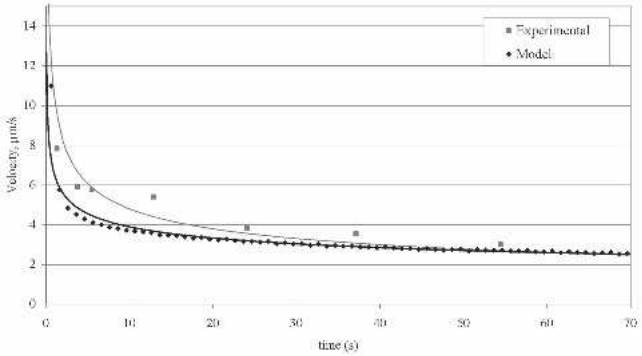

Fig. 13—Austenite/liquid interface velocity, cooling rate = 10 K/min.

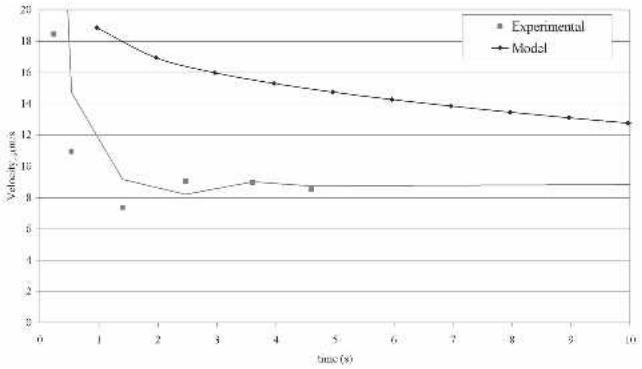

Fig. 14—Austenite/liquid interface velocity, cooling rate = 50 K/min.

reaction at cooling rates of 10 and 50 K/min, respectively. At a cooling rate of 10 K/min, excellent agreement is obtained between the experimental measurements and the simulation. However, at a cooling rate of 50 K/min, the correlation between experimental observations and model predictions is not as close, with the simulation predicting higher transformation rates.

As shown in Figure 13, the experimentally measured velocity of the liquid/austenite interface during the peritectic transformation obeys an exponentially decaying relationship. The first measurement is made after the first second of transformation, at which time a growth rate of 7.8 μm/s is observed. The growth velocity decays to a rate of 3 μm/s after 54 seconds. There is excellent agreement between the experimentally measured growth velocities and model predictions. When the cooling rate is increased to 50 K/min, both the experimentally measured and simulated growth velocities are increased, as shown in Figure 14. However, where the experimentally measured growth velocity attains a rate of 8.5 μm/s over 10 seconds, the simulation predicts that the velocity will be 13 μm/s after 10 seconds. The construction of the simulation domain, as discussed previously, is most likely the primary source of this discrepancy. While at a cooling rate of 100 K/min the experimentally determined growth velocity of the L/γ interface was clearly much higher than that of the γ/δ interface, as shown in Figure 8, it was not possible to conduct a systematic analysis in this instance because the growth velocities were so high that it was impossible to make a sufficient number of measurements.

C. *Model Predictions of the Peritectic Transformation Interface Velocities*

Having benchmarked the model predictions with experimental measurements of the liquid/δ interface, attention is now turned to model predictions of the relative velocities of the L/γ and γ/δ interfaces during the peritectic transformation. The experimental results have clearly indicated that with increased cooling rates, the velocity of both interfaces increases. A "growth inversion" has also been observed at the highest cooling rate, 100 K/min, where the L/γ interface propagates at a rate greater than the γ/δ interface. Model predictions of interface velocity for cooling rates of 10 and 100 K/min will be compared and discussed with reference to the simulated solute profiles that develop during solidification leading to the peritectic transition.

The predicted interface velocities for a cooling rate of 10 K/min are shown in Figure 15 for the time period 10 to 70 seconds. The velocities range from 7.5 to 4.1 μm/s for the solid/solid interface, compared to 4.4 to 2.9 μm/s for the liquid/solid interface at a cooling rate of 10 K/min. This simulation is in line with both the experimental observations made in this study and previous modeling studies. Ha and Hunt,[13] in their numerical analysis of the peritectic transformation, established that the small compositional gap across the solid/solid phase boundaries, in the Ag-Sn system, compared to the gap across the liquid/solid phase boundary, results in the solid/solid interface propagating at a higher rate than the liquid/solid interface. The phase diagram of the Fe-C alloy system has the same shape as that of the Ag-Sn system, and equivalent transformation behavior would therefore be expected. The rationale for this statement is that less solute diffusion is required for the δ to γ transformation than for the L to γ transformation; therefore, it is easier for the solid/solid interface to propagate.

An increase in the cooling rate is expected, quite naturally, to result in an increase in the transformation kinetics and, as shown in Figure 16, the simulated growth rates are higher than at a cooling rate of 10 K/min. The most interesting feature is that the L/γ interface has a higher growth velocity than the γ/δ interface. The growth velocity of the γ/δ interface has a peak value of 20 μm/s and an average of 11 μm/s. The L/γ interface, however, has an initial interfacial growth velocity of 44 μm/s decaying to 24 μm/s. This simulation is in agreement with the *in-situ* observation made in this study that the L/γ can propagate at a higher rate than the γ/δ interface at high cooling rates. In contrast, previous studies and simulations have consistently found that the γ/δ interface grows at a higher rate than the L/γ interface.[9–13]

D. *Solute Profiles and the Peritectic Transformation*

In order to explain the experimentally observed interface velocity inversion and to understand why previous researchers have not been able to predict this behavior, it is necessary to assess the solute profiles that develop as a function of cooling rate. In Figure 17, solute profiles are presented along the central axis of the simulation domain for two cooling conditions, 10 K/min (graphs (a) and (c)) and 100 K/min (graphs (b) and (d)). Graphs (a) and (b) are taken at the time of nucleation of austenite, that is, the austenite is present as a nucleus of near zero diameter and plays no role in the carbon distribution. Graphs (c) and (d) are taken from a nominal subsequent time-step when the peritectic reaction is complete and growth is by the peritectic transformation, and a substantial volume of austenite separates the liquid and delta-ferrite phases.

The solute profile in the liquid phase that develops under a cooling rate of 10 K/min is flatter than the profile that develops at a cooling rate of 100 K/min. This can be explained by the fact that while the concentration limits across the L/δ interface are fixed by the phase diagram, the time available for the diffusion of solute into the liquid is not. Therefore, at a low cooling rate, there is more time for diffusion of solute, leading to a more uniform carbon distribution in the liquid phase, compared to the higher cooling rate.

The development of a steep concentration gradient in the liquid at a cooling rate of 100 K/min has an important implication for the progression of the L/γ interface in the course of the peritectic transformation. The flux of carbon from the austenite to the liquid phase is determined by the diffusion coefficient of the carbon in the liquid and the concentration gradient in the liquid, per Fick's Law. If the development of solute gradients is ignored in a modeling exercise, as is the case under the assumption of complete mixing in the liquid phase, this increased flux of carbon into the liquid, and hence the subsequent increase in the γ/L growth rate, is not taken into account.

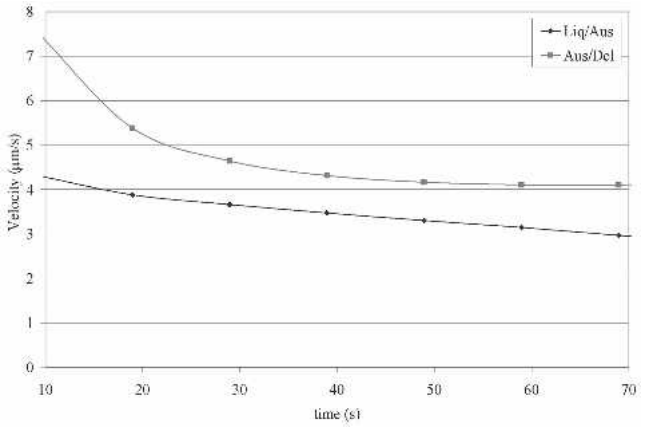

Fig. 15—Simulated interface velocities of the peritectic transformation in an Fe-0.18 mass pct C alloy, cooling rate = 10 K/min.

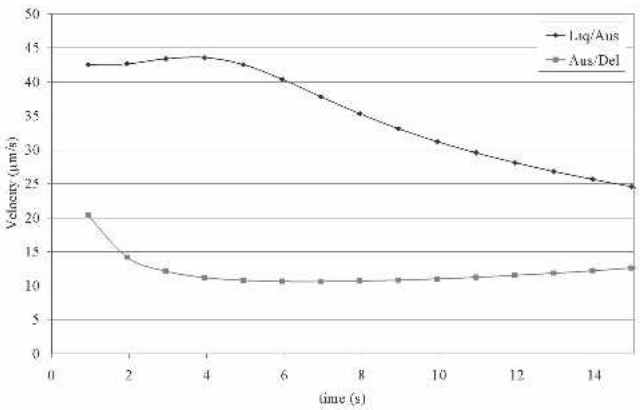

Fig. 16—Simulated interface velocities of the peritectic transformation in an Fe-0.18 mass pct C alloy, cooling rate = 100 K/min.

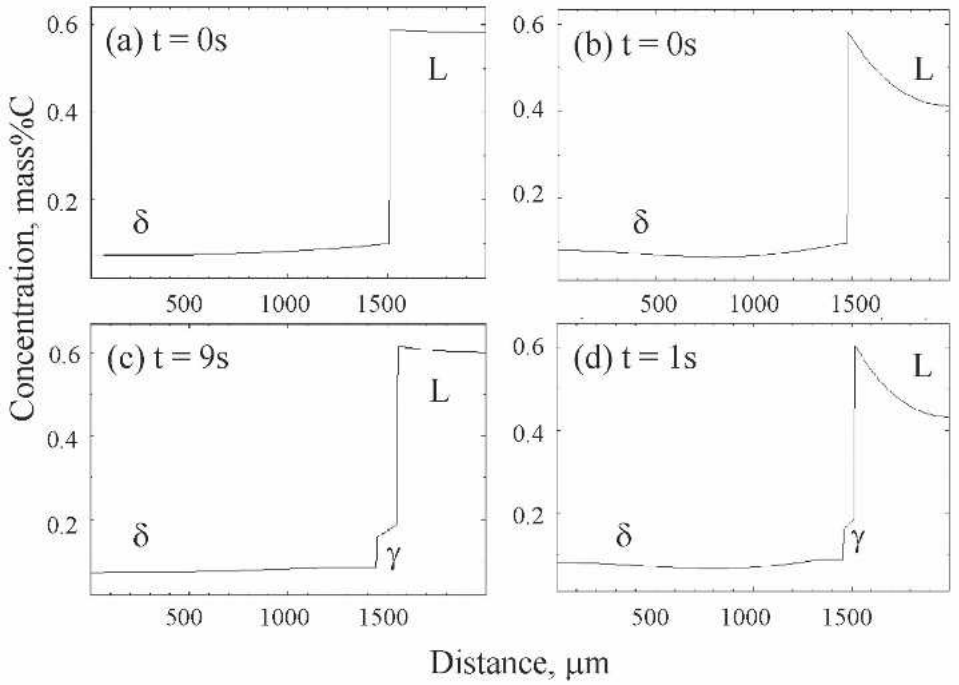

Fig. 17—Comparison of simulation solute profiles for cooling rates of (*a*) and (*c*) 10 K/min and (*b*) and (*d*) 100 K/min, in an Fe-0.18 mass pct C alloy, under a temperature gradient $G = 200$ K/cm; $t = 0$ refers to the initiation of the peritectic phase transition.

In the current study, diffusion in the liquid phase is accounted for in the phase field model simulation, and the predicted L/γ interface velocity increases from 3 to 4 μm/s at a cooling rate of 10 K/min to a value of between 25 and 45 μm/s at a cooling rate of 100 K/min. For the same increase in cooling rate, the δ/γ interface velocity merely increases from 4 to 7 μm/s to 10 to 20 μm/s. Hence, at lower cooling rates, the δ/γ interface grows faster, but at higher cooling rates, the L/γ interface grows faster. This inversion in the rate of propagation of the respective interfaces, predicted by our phase field modeling and observed experimentally, is attributed to enhanced solute flux into the liquid at higher cooling rates due to the presence of a steep solute concentration gradient in the liquid.

VI. CONCLUSIONS

In the current study, in-situ measurements of the kinetics of the peritectic transformation as a function of cooling rate have been compared to predictions, using a multiphase, multicomponent phase field model. Good correlation was found between experimental observations and model predictions. At low cooling rates, the δ/γ interface propagates at a higher rate than the L/γ interface, in agreement with the findings of previous researchers. Conversely, at cooling rates as high as 100 K/min, the L/γ interface propagates at a higher velocity than the δ/γ interface. This inversion, which has been observed experimentally and predicted by the use of a phase field model that takes into account diffusion in the liquid phase, is attributed to solute buildup in the liquid at the L/γ interface. Hence, at increased cooling rates, a significant concentration gradient is established in the liquid at the interface, leading to an increased flux of solute across the interface, culminating in an increased interface propagation velocity.

REFERENCES

1. H.W. Kerr, J. Cisse, and G.F. Bolling: *Acta Metall.*, 1974, vol. 22, pp. 677-86.
2. K. Matsuura, Y. Itoh, and T. Narita: *Iron Steel Inst. Jpn.*, 1993, vol. 33, pp. 583-87.
3. M. El-Bealy and H. Fredriksson: *Metall. Mater. Trans. B*, 1996, vol. 27B, pp. 129-64.
4. H. Yin, T. Emi, and H. Shibata: *Acta Mater.*, 1999, vol. 47, pp. 1523-35.
5. H. Chikama, H. Shibata, T. Emi, and M. Suzuki: *Mater. Trans., JIM*, 1996, vol. 37, pp. 620-26.
6. H. Yin, H. Shibata, T. Emi, and M. Suzuki: *Iron Steel Inst. Jpn.*, 1997, vol. 37, pp. 936-55.
7. H. Shibata, H. Yin, S. Yoshinaga, T. Emi, and M. Suzuki: *Iron Steel Inst. Jpn.*, 1998, vol. 38, pp. 149-56.
8. H. Shibata, H. Yin, and T. Emi: *Phil. Trans. R. Soc. London*, 1998, vol. 356, pp. 957-66.
9. H. Shibata, Y. Arai, M. Suzuki, and T. Emi: *Metall. Mater. Trans. B*, 2000, vol. 31B, pp. 981-91.
10. K. Matsuura, H. Maruyama, Y. Itoh, M. Kudoh, and K. Ishi: *Iron Steel Inst. Jpn.*, 1995, vol. 35, pp. 183-87.
11. A. Das, I. Manna, and S.K. Pabi: *Acta Mater.*, 1999, vol. 47, pp. 1379-88.
12. Y.-M. Won and B.G. Thomas: *Metall. Mater. Trans. A*, 2001, vol. 32A, pp. 1755-76.
13. H.P. Ha and J.D. Hunt: *Metall. Mater. Trans. A*, 2000, vol. 31A, pp. 29-34.
14. J.S. Lee, S.G. Kim, W.T. Kim, and T. Suzuki: *Iron Steel Inst. Jpn.*, 1999, vol. 39, pp. 730-36.
15. D. Phelan and R. Dippenaar: *Proc. Brimacombe Memorial Symp.*, G.A. Irons and A.W. Cramb, eds., Vancouver, 2000, TMS, Warrendale, PA, 2000, pp. 579-93.
16. D.J. Phelan: Ph.D. Thesis, University of Wollongong, Wollongong, 2002.
17. M. Reid, D. Phelan, and R. Dippenaar: *Iron Steel Inst. Jpn.*, 2003, in press.
18. I. Steinbach, F. Pezzolla, B. Nestler, M. Seeßelberg, R. Prieler, G.J. Schmitz, and J.L.L. Rezende: *Physica D*, 1996, vol. 94, pp. 135-47.
19. J. Tiaden: *J. Cryst. Growth*, 1999, vols. 198–199, pp. 1275-80.
20. J. Eiken, M. Apel, B. Böttger, H.J. Diepers, P. Schaffnit, I. Steinbach, and N. Warnken: *3rd Int. Alloy Conf. (IAC-3)*, Estoril, Portugal, June 30–July 5, 2002.
21. W. Kurz and D.J. Fisher: *Fundamentals of Solidification*, 3rd ed., Trans Tech Publications, Aedermannsdorf, Switzerland, 1992, pp. 293-94.